Defect-Free Arbitrary-Geometry Assembly of Mixed-Species Atom Arrays

Cheng Sheng,[1] Jiayi Hou,[1,2] Xiaodong He,[1,*] Kunpeng Wang,[1] Ruijun Guo,[3] Jun Zhuang,[1,2] Bahtiyar Mamat,[1,2] Peng Xu,[1,†] Min Liu,[1] Jin Wang,[1] and Mingsheng Zhan[1]

[1]*State Key Laboratory of Magnetic Resonance and Atomic and Molecular Physics, Wuhan Institute of Physics and Mathematics, Innovation Academy for Precision Measurement Science and Technology, Chinese Academy of Sciences, Wuhan 430071, China*
[2]*School of Physical Sciences, University of Chinese Academy of Sciences, Beijing 100049, China*
[3]*School of Information Engineering and Henan Key Laboratory of Laser and Opto-Electric Information Technology, Zhengzhou University, Zhengzhou 450001, China*

Optically trapped mixed-species single atom arrays with arbitrary geometry are an attractive and promising platform for various applications, because tunable quantum systems with multiple components provide extra degrees of freedom for experimental control. Here, we report the first demonstration of two-dimensional 6×4 dual-species atom assembly of ^{85}Rb (^{87}Rb) atoms with a filling fraction of 0.88 (0.89). This mixed-species atomic synthesis is achieved via rearranging initially randomly distributed atoms by a sorting algorithm (heuristic heteronuclear algorithm) which is designed for bottom-up atom assembly with both user-defined geometries and two-species atom number ratios. Our fully tunable hybrid-atom systems with scalable advantages are a good starting point for high-fidelity quantum logic, many-body quantum simulation, and single molecule array formation.

Single neutral atoms trapped in optical tweezer arrays have been widely used to simulate quantum many-body dynamics [1–9], form cold molecules [10–13], perform quantum logic [14–23] and precisely measure optical frequency [24,25] in recent years. In general, new appealing applications emerge from more degrees of freedom in this experimentally controlled quantum system. For instance, as the number of atoms increases to hundreds, quantum simulators based on Rydberg atom arrays can solve quantum many-body problems which are intractable on classical machines [7–9]. Moreover, three-dimensional quantum annealers with the adjustable connectivity of atoms hold promise for quantum optimization problems [5,6]. These various applications are demonstrated on single-species defect-free atom arrays, while mixed-species atom assembly should be a more versatile platform in the future.

For quantum logic, ion systems benefit greatly from the use of dual-species ions, one for data ions and another for ancilla ions [26–30]. Otherwise, decoherence of the data ions occurs when absorbing photons re-emitted by measurement or sympathetic cooling process of ancilla ions if they are identical [31]. Akin to trapped ions, the implements of high-fidelity quantum logic on the neutral atom platforms can also be impeded by these problems. Therefore, with the previous demonstration of the entanglement of two different isotopes atoms via Rydberg blockade [18], a dual-species neutral atom array is essential to realize schemes, such as nondestructive cooling via Rydberg interactions [32], nondemolition state measurement with low cross-talk [33], and surface code for quantum error correction [34,35].

On the other hand, optically trapped single molecules are directly laser cooled [36] or formed by two single atoms [10–13,37,38]. In the optical lattice, while the conversion efficiency from a pair of atoms in one site to a Feshbach molecule via magneto-association can reach about 90%, the overall filling fraction of cold molecules is limited to 25%–30% due to the relatively low preparation efficiency of dual-species atom pairs in one site [37,38]. In recent years, merging two single atoms in optical tweezers has been developed to build single molecules [10–13]. Along this way, bottom-up defect-free dual-species atom arrays could be an excellent starting point for generating ultracold single molecule arrays with high filling fractions.

Multispecies may also provide flexibility to control the interaction between atoms for quantum simulations [39,40]. With such versatile applications, dual-species atom array would become a promising platform for quantum computation, quantum simulation and single molecule arrays. So far, single-species defect-free atom arrays have been well prepared from one dimension to three dimensions [41–50]. However, the generation of mixed-species defect-free atom arrays has not been reported yet by both bottom-up and top-down approaches.

Here, we present a realization of preparing two-dimensional dual-isotope atom (^{85}Rb and ^{87}Rb) arrays with arbitrary geometries. The defect-free atom assembly is formed by rearranging the randomly distributed atoms using our heuristic heteronuclear algorithm (HHA) which
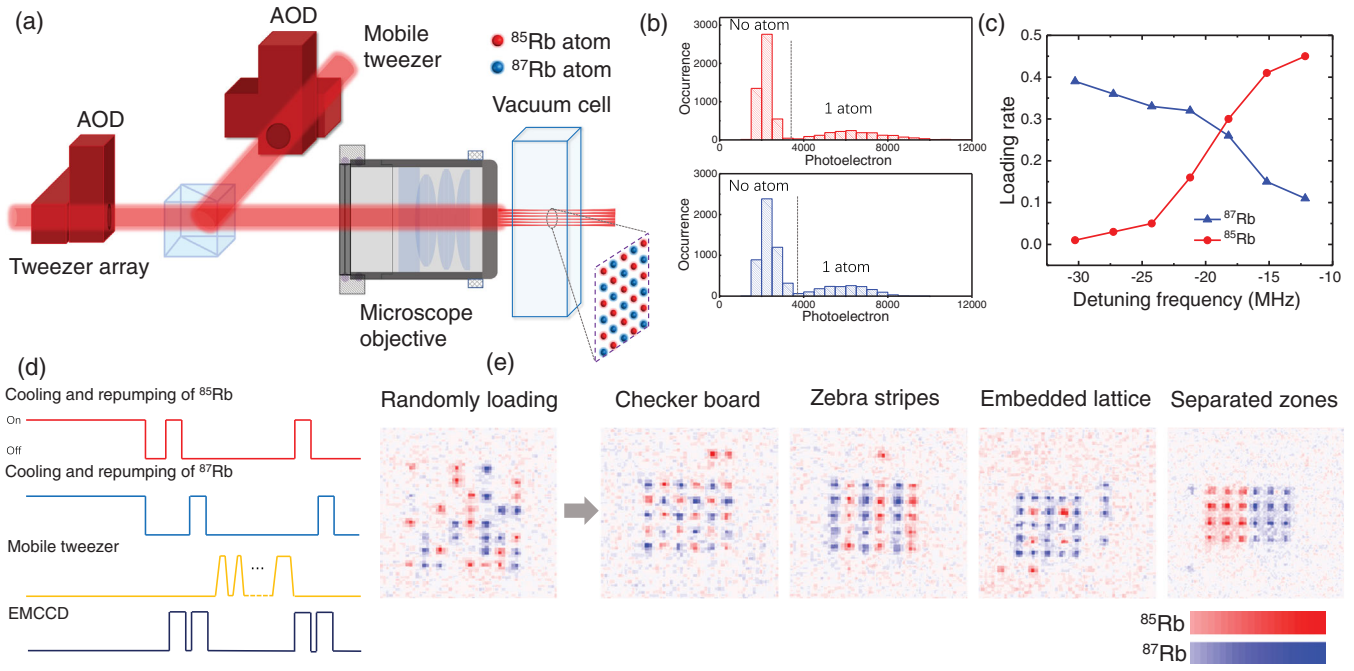
FIG. 1.   Protocol for creating mixed-species atom array. (a) Simplified schematics of the experimental setup. (b) Fluorescence count distribution for 64 tweezers during 80 ms of exposure of ^{85}Rb (top) and ^{87}Rb (down) atoms. (c) The loading rates of ^{85}Rb and ^{87}Rb as a function of the frequency of ^{85}Rb cooling beam. The frequency of ^{87}Rb cooling beam is fixed to 15 MHz detuned by $|5S_{1/2}, F = 2\rangle \rightarrow |5P_{3/2}, F = 3\rangle$ and the loading ratios are tuned by the frequency of ^{85}Rb cooling beam detuned by $|5S_{1/2}, F = 3\rangle \rightarrow |5P_{3/2}, F = 4\rangle$. The optical intensity of ^{85}Rb and ^{87}Rb cooling (repumping) beams are almost the same. The frequency value is set to the intersection of the two lines when we prepare the atom arrays with equal ^{85}Rb and ^{87}Rb atom numbers. The tunability is also essential for arrays with imbalanced two-species atom numbers such as "embedded lattice" configuration. (d) Pulse diagram of the experimental sequence. (e) Images of various defect-free mixed-species atom arrays. Each one is synthesized by one image of ^{85}Rb atoms and one image of ^{87}Rb atoms. The distance of the neighboring sites is 5 μm.

is designed for compact dual-species atom assembly with user-defined configurations. The measured filling fraction of 6×4 atom assembly of ^{87}Rb (^{85}Rb) atoms is 0.89 (0.88), which is mainly limited by the atom survival probability in optical tweezers. After the sorting atom process, the configuration entropy of the dual-species atom system is lowered by a factor of 5.

Our experimental setup is shown schematically in Fig. 1(a) (details in Ref. [50]). In brief, the 808-nm 8×8 tweezer array is generated by an acousto-optic deflector (AOD) driven by a multitone radio-frequency (rf) and the trap depth of each tweezer is about $U_0/k_B \approx 0.8$ mK, where k_B is the Boltzmann constant. To efficiently transport atoms, an 830-nm mobile tweezer with a deeper trap depth of 2.3 mK is created by another AOD driven by a dynamically controlled rf. First, the dual-species single atoms are stochastically loaded into the tweezer array from an overlapped magneto-optical trap of ^{85}Rb and ^{87}Rb with a total loading rate about 50% in 950 ms. The light-assisted collisions between heteronuclear atoms allow us to control the two-species atom loading ratio by tuning the frequencies of ^{85}Rb and ^{87}Rb cooling lasers. The recorded loading rate as a function of the detuning frequencies of ^{85}Rb is plotted in Fig. 1(c).

The images of ^{85}Rb and ^{87}Rb atom fluorescence are taken by an electron multiplying charge-coupled device (EMCCD) camera to reveal their initial positions in the atom arrays. The photoelectron count thresholds as shown in Fig. 1(b) and the regions of interest of ^{85}Rb and ^{87}Rb atoms for every tweezer are respectively calibrated via automatically analyzing a series of atom array images. Then, according to the two initial images of ^{85}Rb and ^{87}Rb detected, respectively, by their fluorescence and the user-defined target sites, the HHA is used to calculate the sorting-atom path of the mobile tweezer. The sorting-atom path is composed of a list of voltage sequences to control the optical intensity and X and Y positions of the mobile tweezer. Rearrangement of one atom (also defined as one move) involves extracting the atom by the mobile tweezer, moving the mobile tweezer along a calculated path, and releasing the atom onto a target site. Finally, after the rearrangement for all atoms are accomplished, the new images of ^{85}Rb and ^{87}Rb atom array are acquired as illustrated in Fig. 1(e). The total experimental process sequence is depicted in Fig. 1(d).

Dual-species atom arrays in specific patterns as illustrated in Fig. 1(e) have their designed purpose. For instance, "checker board" configuration is suited for
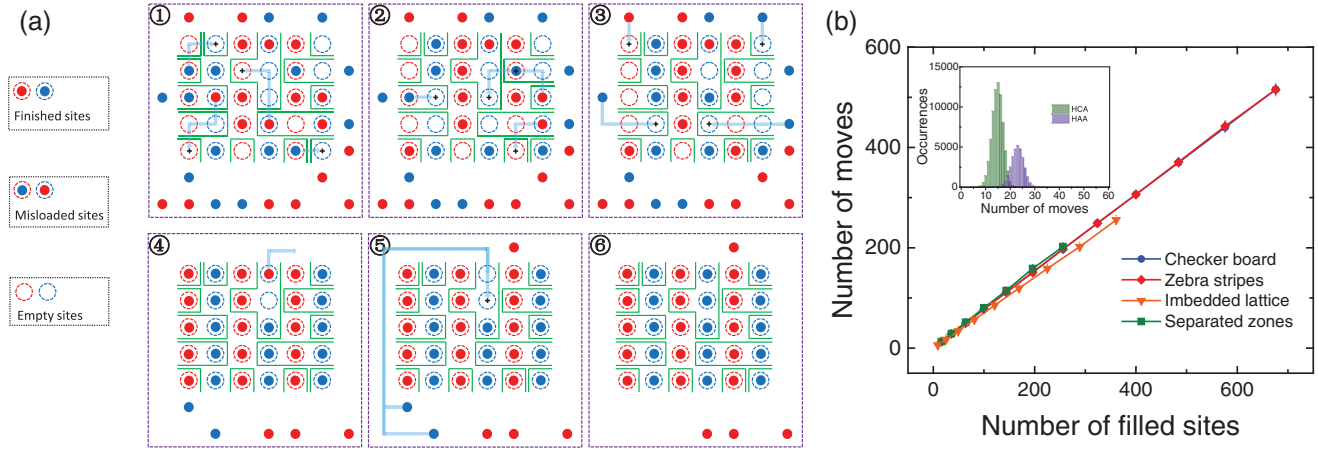
FIG. 2. Assembling of a mixed-species atom array using the HHA. (a) Schematic diagrams of the HHA. The sorting process is from left to right. The blue (red) disks denote single atoms of ^{87}Rb (^{85}Rb) and the blue (red) dashed line circles denote the target sites of ^{87}Rb (^{85}Rb). The green regions represent the routes connected to the reservoir tweezers and the sites with "+" symbols are the innermost sites in the routes to be filled. (b) The number of moves as a function of the number of filled sites for dual-species atom arrays. The averaged simulation results are repeated by 100 000 times with randomly initial configurations for the $N \times N$ arrays, which are enlarged by increasing the N. The inset shows the histogram of the number of moves of preparing a 5×6 single-species atom array and a 5×6 dual-species atom array in zebra stripes configuration.

surface code, one for data qubits, the other one for measurement qubits [34,35] or the scheme proposed for quantum nondemolition state measurements based on Rydberg interaction [33]. In addition, substantially different resonant frequencies of the dual-species atom allow us to individually address qubits in a closely spaced atom array with low cross-talk via addressing laser beams. "Zebra stripes" configuration is prepared for building single molecule arrays. The neighboring two columns of two-species atoms can be merged into one column of the two-atom reservoirs. Atom pairs then can be converted to single molecules by means of photo-association, Feshbach resonance or spin-motion coupling [10–13].

The distance of the neighboring sites allows us to move the atoms between adjacent site rows or along the links of the sites. The latter way requires the moving to avoid the filled sites, and the corresponding sorting-atom algorithm is much complex. But such a moving way is typically required for scaling up compact tweezer arrays [7,48,51]. In the condition that optical tweezers can trap both two-species atoms and atoms are moved along the site links, a sorting-atom algorithm applicable to dual-species atom arrays is much more complicated than single-species atom algorithm. Because the occurrence of misplaced atoms (for example, a ^{85}Rb target site is occupied with a ^{87}Rb atom) is difficult to deal with. To solve this problem, we propose a heuristic sorting-atom algorithm (HHA) with near-fewest sorting-atom moves to rearrange dual-species atoms into compact target configurations for bottom-up atom assembly. A brief introduction of the working principle is shown in Fig. 2(a). First of all, we classify the target sites into finished sites and unfinished sites after the initial loading process. The finished sites have already been filled

with target atoms. Atoms in these sites will not be moved during the whole rearrangement. The unfinished sites include misloaded sites and empty sites, where the misloaded sites are filled with the misplaced atoms. Next, the unfinished sites are divided into several groups. Each group starts from an outermost unfinished site, then connects the adjacent unfinished sites step by step until all unfinished sites are included in the groups as the green region in Fig. 2(a) shown. In this way, the unfinished sites then can be efficiently filled in order.

After all the sites are classified and grouped, two types of atoms are used to fill the unfinished sites. The type-M atoms are the misplaced atoms in the target region and the type-R atoms are the reservoir atoms in the outside region (sites in the nontarget region). First, the innermost empty sites of each group are filled with the nearest type-M atoms where the routes connecting them do not have any obstacle atoms. When this process is accomplished once, some misloaded sites are converted to the empty sites. Then, a repeated process is carried out to fill the new empty sites. After several cycles, most of the innermost empty sites become finished sites. Next, the second (third and so on) innermost sites are filled in the same way. The rest of empty sites due to a lack of the type-M source atoms turn to search the nearest type-R source atoms to become unit filling as the third step in Fig. 2(a) illustrated. The type-M atoms that cannot be used to fill empty sites due to the blocked sorting-atom path are transported to the empty reservoir tweezers in the outside region. Finally, the remaining empty sites caused by removing the redundant type-M atoms are also filled with the type-R source atoms. The calculation success rates and the flowchart of the HHA are described in the Supplemental Material [52].

Previously, we have noted that the filling fraction is affected by the number of moves [49,50]. Therefore, the primary purpose to design the HHA is reducing the moves as few as possible. The inset in Fig. 2(b) shows that the HHA costs more number of moves compared with heuristic cluster algorithm (HCA). HCA is algorithm with near fewest sorting-atom moves for single-species atom arrays that has been described in Ref. [50]. This is mainly resulted from the transport of misplaced atoms which does not occur in the single-species atom arrays. Another reason is that about only 25% target sites in dual-species atom arrays are initially finished, while 50% sites are filled in single-species atom arrays as usual. Nevertheless, the number of moves of the HHA is still optimal, even smaller than some algorithms of the single-species atom arrays. Additionally, the HHA gives a linear relation between number of moves and that of filled sites in four configurations as shown in Fig. 2(b). This indicates that the HHA is well suited for larger-scale dual-species atom arrays [49,50].

Analyzing 100 repetitions of the experiment for mixed-species atom arrays in zebra stripes configuration, the filling fractions of ^{85}Rb and ^{87}Rb target sites are measured as the number of atom pairs is increased [Fig. 3(a)]. We achieve a preparation of 12 dual-species atom pairs with a filling fraction of 0.89(2) for ^{87}Rb and 0.88(2) for ^{85}Rb after one arrangement cycle. As the inset shows in Fig. 3(a), our method significantly improves the cumulative success rates (the probability of preparing an entire defect-free array) of the mixed-species atom array. The experimental filling fractions are mainly limited by the atom preservation efficiency in the tweezer array. The preservation efficiencies of ^{87}Rb and ^{85}Rb are measured to be 92% and 94%, respectively, when the rearrangement process is not implemented. The atom loss is induced by the heating in the probing atom process and the background gas collisions (preservation efficiencies > 99% has been achieved at cryogenic environment [51]). Another factor that affects the filling fraction is the atom transport efficiency (about 98% in our experiment and typically 98%–99% at most [49]), but the experimental imperfections in the transport process can be mitigated by rearranging the atom array for several cycles. Also, compared with preparation of single-species array, needing more moves to prepare dual-species arrays leads to lower filling fractions. The filling fractions differ little for the above four configurations due to their close number of moves during the rearrangement [Fig. 2(b)]. Moreover, the array size can be further increased to about one hundred only requiring sufficient laser power for reliable atom trapping with no more changes in other hardware.

Moreover, we measure the configuration entropy during rearrangement in a frame of Maxwell's demon like as depicted in Fig. 3(b). The entropy per particle in each region is defined as [52]
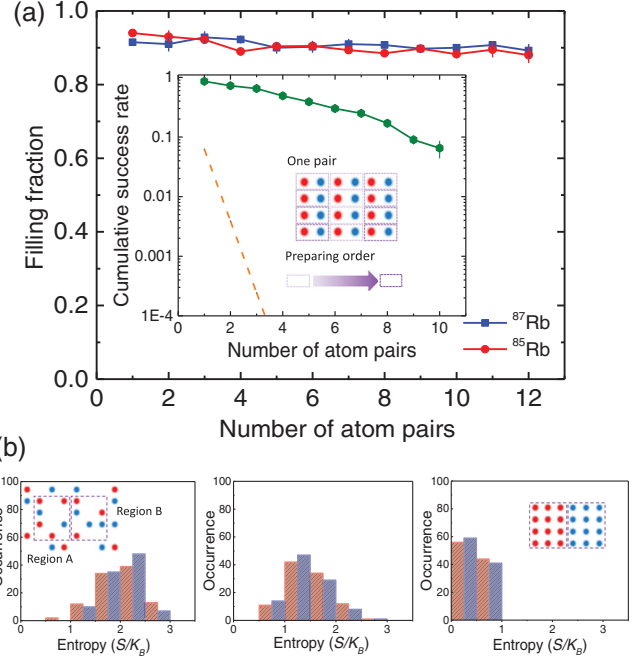

FIG. 3. Filling fraction and configuration entropy of the dual-species atom array. (a) Filling fraction of ^{85}Rb and ^{87}Rb as a function of the number of atom pairs. Inset: Green circles show the cumulative success rate of obtaining a defect-free atom array with several atom pairs; the dashed line shows the result corresponding to random loading for dual-species atoms. The cumulative success rates $P_n = 2^{-2n}$ for randomly loading dual-species array, where n is the number of filled sites, if the loading ratios are 25% for both two-species atoms. The number of atom pairs is accumulated through a path marked by the color gradient of purple dashed rectangles. (b) Configuration entropy decreasing in the process of rearrangement. Each entropy distribution is measured by repeating the experiment for 100 times. The left (right) one is the result of initial (final) atom array and the red (blue) one is the result of region A (B). The middle one represents the entropy with half of the total transport moves. The values of entropy during the sorting process in region A and B are 2.0(5), 1.5(4), 0.4(3)k_B and 2.0(4), 1.4(4), 0.4(2)k_B, respectively.

$$S = -\frac{k_B}{n+m}[n\ln n + m\ln m + (1-n-m)\ln(1-n-m)],$$

(1)

where $n(m)$ is the filling fraction of ^{85}Rb (^{87}Rb) atoms in this target region. In this microscopic system with the initial configurational disorder, the entropy is reduced by the sorting atom process. A factor of 5 for lowering the entropy is achieved. In fact, an information entropy is increased when our demon acquires the atom occupancy of the whole system and map out a plan to act on all the particles. Therefore, the second law of thermodynamics is not violated by the lowering entropy process. The configuration entropy of the final atom array is not zero because each region cannot reach unit filling due to the technical

imperfections. Additionally, the vibrational entropy can also be decreased if we adopt the method of dual-species Raman sideband cooling as in our previous experiment [53].

In summary, we have presented a novel platform of configurable defect-free different isotopes atom assembly. This approach can also be applied to some cases of preparing dual-element atom array. The working condition is that the optical tweezers in the array are the attractive potential traps for both two-species atoms [52]. The bottom-up mixed-species atom array opens promising paths to realizing fault-tolerant logic quantum bits with low cross-talk, ultracold single molecule arrays with high filling fractions, and quantum many-body simulations with site-specific manipulations illuminated by global Rydberg-excitation beams.

---

*hexd@wipm.ac.cn
†etherxp@wipm.ac.cn

[1] H. Bernien, S. Schwartz, A. Keesling, H. Levine, A. Omran, H. Pichler, S. Choi, A. S. Zibrov, M. Endres, M. Greiner, V. Vuletić, and M. D. Lukin, Probing many-body dynamics on a 51-atom quantum simulator, Nature (London) **551**, 579 (2017).

[2] V. Lienhard, S. de Léséleuc, D. Barredo, T. Lahaye, A. Browaeys, M. Schuler, L.-P. Henry, and A. M. Läuchli, Observing the Space- and Time-Dependent Growth of Correlations in Dynamically Tuned Synthetic Ising Models with Antiferromagnets, Phys. Rev. X **8**, 021070 (2018).

[3] A. Keesling, A. Omran, H. Levine, H. Bernien, H. Pichler, S. Choi, R. Samajdar, S. Schwartz, P. Silvi, S. Sachdev, P. Zoller, M. Endres, M. Greiner, V. Vuletić, and M. D. Lukin, Quantum Kibble-Zurek mechanism and critical dynamics on a programmable Rydberg simulator, Nature (London) **568**, 207 (2019).

[4] S. de Léséleuc, V. Lienhard, P. Scholl, D. Barredo, S. Weber, N. Lang, H. P. Büchler, T. Lahaye, and A. Browaeys, Observation of a symmetry-protected topological phase of interacting bosons with Rydberg atoms, Science **365**, 775 (2019).

[5] M. Kim, Y. Song, J. Kim, and J. Ahn, Quantum Ising Hamiltonian programming in trio, quartet, and sextet qubit systems, PRX Quantum **1**, 020323 (2020).

[6] Y. Song, M. Kim, H. Hwang, W. Lee, and J. Ahn, Quantum simulation of Cayley-tree Ising Hamiltonians with three-dimensional Rydberg atoms, Phys. Rev. Research **3**, 013286 (2021).

[7] S. Ebadi, T. T. Wang, H. Levine, A. Keesling, G. Semeghini, A. Omran, D. Bluvstein, R. Samajdar, H. Pichler, W. W. Ho, S. Choi, S. Sachdev, M. Greiner, V. Vuletić, and M. D. Lukin, Quantum phases of matter on a 256-atom programmable quantum simulator, Nature (London) **595**, 227 (2021).

[8] P. Scholl, M. Schuler, H. J. Williams, A. A. Eberharter, D. Barredo, K.-N. Schymik, V. Lienhard, L.-P. Henry, T. C. Lang, T. Lahaye, A. M. Läuchli, and A. Browaeys, Quantum simulation of 2D antiferromagnets with hundreds of Rydberg atoms, Nature (London) **595**, 233 (2021).

[9] D. Bluvstein, A. Omran, H. Levine, A. Keesling, G. Semeghini, S. Ebadi, T. T. Wang, A. A. Michailidis, N. Maskara, W. W. Ho, S. Choi, M. Serbyn, M. Greiner, V. Vuletić, and M. D. Lukin, Controlling quantum many-body dynamics in driven Rydberg atom arrays, Science **371**, 1355 (2021).

[10] L. R. Liu, J. D. Hood, Y. Yu, J. T. Zhang, N. R. Hutzler, T. Rosenband, and K.-K. Ni, Building one molecule from a reservoir of two atoms, Science **360**, 900 (2018).

[11] L. R. Liu, J. D. Hood, Y. Yu, J. T. Zhang, K. Wang, Y.-W. Lin, T. Rosenband, and K.-K. Ni, Molecular Assembly of Ground-State Cooled Single Atoms, Phys. Rev. X **9**, 021039 (2019).

[12] J. T. Zhang, Y. Yu, W. B. Cairncross, K. Wang, L. R. B. Picard, J. D. Hood, Y.-W. Lin, J. M. Hutson, and K.-K. Ni, Forming a Single Molecule by Magnetoassociation in an Optical Tweezer, Phys. Rev. Lett. **124**, 253401 (2020).

[13] X. He, K. Wang, J. Zhuang, P. Xu, X. Gao, R. Guo, C. Sheng, M. Liu, J. Wang, J. Li, G. V. Shlyapnikov, and M. Zhan, Coherently forming a single molecule in an optical trap, Science **370**, 331 (2020).

[14] T. Xia, M. Lichtman, K. Maller, A. W. Carr, M. J. Piotrowicz, L. Isenhower, and M. Saffman, Randomized Benchmarking of Single-Qubit Gates in a 2D Array of Neutral-Atom Qubits, Phys. Rev. Lett. **114**, 100503 (2015).

[15] M. Saffman, Quantum computing with atomic qubits and Rydberg interactions: Progress and challenges, J. Phys. B **49**, 202001 (2016).

[16] J. Yang, X. He, R. Guo, P. Xu, K. Wang, C. Sheng, M. Liu, J. Wang, A. Derevianko, and M. Zhan, Coherence Preservation of a Single Neutral Atom Qubit Transferred Between Magic-Intensity Optical Traps, Phys. Rev. Lett. **117**, 123201 (2016).

[17] Y. Wang, A. Kumar, T. Wu, and D. S. Weiss, Single-qubit gates based on targeted phase shifts in a 3D neutral atom array, Science **352**, 1562 (2016).

[18] Y. Zeng, P. Xu, X. He, Y. Liu, M. Liu, J. Wang, D. J. Papoular, G. V. Shlyapnikov, and M. Zhan, Entangling Two Individual Atoms of Different Isotopes via Rydberg Blockade, Phys. Rev. Lett. **119**, 160502 (2017).

[19] C. Sheng, X. He, P. Xu, R. Guo, K. Wang, Z. Xiong, M. Liu, J. Wang, and M. Zhan, High-Fidelity Single-Qubit Gates on Neutral Atoms in a Two-Dimensional Magic-Intensity Optical Dipole Trap Array, Phys. Rev. Lett. **121**, 240501 (2018).

[20] H. Levine, A. Keesling, G. Semeghini, A. Omran, T. T. Wang, S. Ebadi, H. Bernien, M. Greiner, V. Vuletić,

H. Pichler, and M. D. Lukin, Parallel Implementation of High-Fidelity Multiqubit Gates with Neutral Atoms, Phys. Rev. Lett. **123**, 170503 (2019).

[21] T. M. Graham, M. Kwon, B. Grinkemeyer, Z. Marra, X. Jiang, M. T. Lichtman, Y. Sun, M. Ebert, and M. Saffman, Rydberg-Mediated Entanglement in a Two-Dimensional Neutral Atom Qubit Array, Phys. Rev. Lett. **123**, 230501 (2019).

[22] R. Guo, X. He, C. Sheng, J. Yang, P. Xu, K. Wang, J. Zhong, M. Liu, J. Wang, and M. Zhan, Balanced Coherence Times of Atomic Qubits of Different Species in a Dual 3×3 Magic-Intensity Optical Dipole Trap Array, Phys. Rev. Lett. **124**, 153201 (2020).

[23] I. S. Madjarov, J. P. Covey, A. L. Shaw, J. Choi, A. Kale, A. Cooper, H. Pichler, V. Schkolnik, J. R. Williams, and M. Endres, High-fidelity entanglement and detection of alkaline-earth Rydberg atoms, Nat. Phys. **16**, 857 (2020).

[24] M. A. Norcia, A. W. Young, W. J. Eckner, E. Oelker, J. Ye, and A. M. Kaufman, Seconds-scale coherence on an optical clock transition in a tweezer array, Science **366**, 93 (2019).

[25] A. W. Young, W. J. Eckner, W. R. Milner, D. Kedar, M. A. Norcia, E. Oelker, N. Schine, J. Ye, and A. M. Kaufman, Half-minute-scale atomic coherence and high relative stability in a tweezer clock, Nature (London) **588**, 408 (2020).

[26] P. O. Schmidt, T. Rosenband, C. Langer, W. M. Itano, J. C. Bergquist, and D. J. Wineland, Spectroscopy using quantum logic, Science **309**, 749 (2005).

[27] T. R. Tan, J. P. Gaebler, Y. Lin, Y. Wan, R. Bowler, D. Leibfried, and D. J. Wineland, Multi-element logic gates for trapped-ion qubits, Nature (London) **528**, 380 (2015).

[28] C. J. Ballance, V. M. Schäfer, J. P. Home, D. J. Szwer, S. C. Webster, D. T. C. Allcock, N. M. Linke, T. P. Harty, D. P. L. A. Craik, D. N. Stacey, A. M. Steane, and D. M. Lucas, Hybrid quantum logic and a test of Bell's inequality using two different atomic isotopes, Nature (London) **528**, 384 (2015).

[29] V. Negnevitsky, M. Marinelli, K. K. Mehta, H.-Y. Lo, C. Flühmann, and J. P. Home, Repeated multi-qubit readout and feedback with a mixed-species trapped-ion register, Nature (London) **563**, 527 (2018).

[30] K. Sosnova, A. Carter, and C. Monroe, Character of motional modes for entanglement and sympathetic cooling of mixed-species trapped-ion chains, Phys. Rev. A **103**, 012610 (2021).

[31] C. D. Bruzewicz, J. Chiaverini, R. McConnell, and J. M. Sage, Trapped-ion quantum computing: Progress and challenges, Appl. Phys. Rev. **6**, 021314 (2019).

[32] R. Belyansky, J. T. Young, P. Bienias, Z. Eldredge, A. M. Kaufman, P. Zoller, and A. V. Gorshkov, Nondestructive Cooling of an Atomic Quantum Register via State-Insensitive Rydberg Interactions, Phys. Rev. Lett. **123**, 213603 (2019).

[33] I. I. Beterov and M. Saffman, Rydberg blockade, Förster resonances, and quantum state measurements with different atomic species, Phys. Rev. A **92**, 042710 (2015).

[34] A. G. Fowler, M. Mariantoni, J. M. Martinis, and A. N. Cleland, Surface codes: Towards practical large-scale quantum computation, Phys. Rev. A **86**, 032324 (2012).

[35] J. M. Auger, S. Bergamini, and D. E. Browne, Blueprint for fault-tolerant quantum computation with Rydberg atoms, Phys. Rev. A **96**, 052320 (2017).

[36] L. Anderegg, L. W. Cheuk, Y. Bao, S. Burchesky, W. Ketterle, K.-K. Ni, and J. M. Doyle, An optical tweezer array of ultracold molecules, Science **365**, 1156 (2019).

[37] L. Reichsöllner, A. Schindewolf, T. Takekoshi, R. Grimm, and H.-C. Nägerl, Quantum Engineering of a Low-Entropy Gas of Heteronuclear Bosonic Molecules in an Optical Lattice, Phys. Rev. Lett. **118**, 073201 (2017).

[38] S. A. Moses, J. P. Covey, M. T. Miecnikowski, B. Yan, B. Gadway, J. Ye, and D. S. Jin, Creation of a low-entropy quantum gas of polar molecules in an optical lattice, Science **350**, 659 (2015).

[39] H. Weimer, M. Müller, I. Lesanovsky, P. Zoller, and H. P. Büchler, A Rydberg quantum simulator, Nat. Phys. **6**, 382 (2010).

[40] A. Browaeys and T. Lahaye, Many-body physics with individually controlled Rydberg atoms, Nat. Phys. **16**, 132 (2020).

[41] H. Kim, W. Lee, H.-G. Lee, H. Jo, Y. Song, and J. Ahn, In situ single-atom array synthesis using dynamic holographic optical tweezers, Nat. Commun. **7**, 13317 (2016).

[42] M. Endres, H. Bernien, A. Keesling, H. Levine, E. R. Anschuetz, A. Krajenbrink, C. Senko, V. Vuletić, M. Greiner, and M. D. Lukin, Atom-by-atom assembly of defect-free one-dimensional cold atom arrays, Science **354**, 1024 (2016).

[43] D. Barredo, S. Léséleuc, V. Lienhard, T. Lahaye, and A. Browaeys, An atom-by-atom assembler of defect-free arbitrary two-dimensional atomic arrays, Science **354**, 1021 (2016).

[44] W. Lee, H. Kim, and J. Ahn, Defect-free atomic array formation using the Hungarian matching algorithm, Phys. Rev. A **95**, 053424 (2017).

[45] D. Barredo, V. Lienhard, S. de Léséleuc, T. Lahaye, and A. Browaeys, Synthetic three-dimensional atomic structures assembled atom by atom, Nature (London) **561**, 79 (2018).

[46] A. Kumar, T. Wu, F. Giraldo, and D. S. Weiss, Sorting ultracold atoms in a three-dimensional optical lattice in a realization of Maxwell's demon, Nature (London) **561**, 83 (2018).

[47] M. O. Brown, T. Thiele, C. Kiehl, T.-W. Hsu, and C. A. Regal, Gray-Molasses Optical-Tweezer Loading: Controlling Collisions for Scaling Atom-Array Assembly, Phys. Rev. X **9**, 011057 (2019).

[48] D. O. de Mello, D. Schäffner, J. Werkmann, T. Preuschoff, L. Kohfahl, M. Schlosser, and G. Birkl, Defect-Free Assembly of 2D Clusters of More Than 100 Single-Atom Quantum Systems, Phys. Rev. Lett. **122**, 203601 (2019).

[49] K.-N. Schymik, V. Lienhard, D. Barredo, P. Scholl, H. Williams, A. Browaeys, and T. Lahaye, Enhanced atom-by-atom assembly of arbitrary tweezers arrays, Phys. Rev. A **102**, 063107 (2020).

[50] C. Sheng, J. Hou, X. He, P. Xu, K. Wang, J. Zhuang, X. Li, M. Liu, J. Wang, and M. Zhan, Efficient preparation of two-dimensional defect-free atom arrays with near-fewest sorting-atom moves, Phys. Rev. Research **3**, 023008 (2021).

[51] K.-N. Schymik, S. Pancaldi, F. Nogrette, D. Barredo, J. Paris, A. Browaeys, and T. Lahaye, Single Atoms with 6000-Second Trapping Lifetimes in Optical-Tweezer Arrays at Cryogenic Temperatures, Phys. Rev. Applied **16**, 034013 (2021).

[52] See Supplemental Material at http://link.aps.org/supplemental/10.1103/PhysRevLett.128.083202 for the calculation success rates of the HHA, the flowchart of the HHA, the definition of the configuration entropy of mutiple-species atom arrays, and for the scheme of dual-element atom arrays.

[53] K. Wang, X. He, R. Guo, P. Xu, C. Sheng, J. Zhuang, Z. Xiong, M. Liu, J. Wang, and M. Zhan, Preparation of a heteronuclear two-atom system in the three-dimensional ground state in an optical tweezer, Phys. Rev. A **100**, 063429 (2019).